Overpressure generating mechanisms in the Peciko Field, Lower Kutai Basin, Indonesia

Agus M. Ramdhan[1*] and Neil R. Goulty[1]

[1]*Department of Earth Sciences, Durham University, South Road, Durham DH1 3LE, UK*

**Corresponding author (e-mail: a.m.ramdhan@dur.ac.uk)*

Running title: Overpressure generating mechanisms in the Peciko Field

ABSTRACT: The Peciko Field contains gas in multiple stacked reservoirs within a Miocene deltaic sequence. In the deeper reservoirs, gas is trapped hydrodynamically by high lateral overpressure gradients. We have analysed overpressure and compaction in this field by using wireline log, pressure, temperature, and vitrinite reflectance data. The top of overpressure is located below 3 km burial depth, below the depth range for transformation of discrete smectite to mixed-layer illite/smectite. Density-sonic and density-resistivity crossplots for mudrocks show reversals within the transition zone into hard overpressure below 3.5 km depth. Vitrinite reflectance measurements indicate that the start of unloading coincides with the onset of gas generation. Moreover, mudrock density continues to increase with depth in the overpressured section to values above 2.6 g cm^{-3}. We conclude that gas generation and chemical compaction are responsible for overpressure generation, contradicting previous interpretations that disequilibrium compaction is the principal mechanism for generating overpressure in the Lower Kutai Basin. The particular circumstances which make our radical interpretation plausible are that it is a warm basin with lateral reservoir drainage, so the overpressured mudrocks are probably overcompacted as a result of diagenesis.

KEYWORDS: *Lower Kutai Basin, overpressure, unloading, gas generation, compaction*

Introduction

Overpressure in Cenozoic basins is commonly associated with the inability of fluid to escape rapidly enough to remain in hydrostatic equilibrium during ongoing burial. As a consequence, the sediments retain higher porosities than they would do if the pore pressure were hydrostatic. This process is referred to as disequilibrium compaction (Swarbrick *et al*. 2002). Disequilibrium compaction was recognized as a primary mechanism for generating overpressure in the US Gulf Coast region over 40 years ago (Pennebaker 1968; Reynolds 1970). Since then, disequilibrium compaction has been diagnosed as the cause of overpressure in many sedimentary basins worldwide, including the Neogene prodelta mudrocks of the Baram Delta, Brunei (Tingay *et al.* 2009).

More recent work in overpressure analysis has shown the importance of other overpressure generating mechanisms apart from disequilibrium compaction, even in Neogene sequences. These overpressure generating mechanisms, such as gas generation, clay diagenesis, aquathermal pressuring and pressure transference, can be classified as unloading mechanisms (Bowers 1995). Some examples of basins where these mechanisms have been shown to be active are Haltenbanken and the Northern North Sea (Hermanrud *et al*. 1998; Teige *et al*. 1999, 2007), the Eugene Island area of the Gulf of Mexico (Bowers 2001), and the inner shelf sequence of the Baram Delta (Tingay *et al*. 2009).

The Peciko Field is located within Miocene strata in the Lower Kutai Basin, Kalimantan, Indonesia (Fig. 1). A transition zone into hard overpressure is encountered in the field at depths of 11,000–14,000 ft (3350–4250 m). The primary mechanism responsible for overpressure generation in this area has previously been interpreted to be disequilibrium compaction (Bois *et al*. 1994; Bates 1996; Burrus 1998).

The principal objective of the work reported here was to determine whether disequilibrium compaction really is the mechanism responsible for generating overpressure in the Peciko Field. A secondary aim was to find a method which can be used during drilling mudrock sections to estimate overpressure for wider application in the basin. By analysing wireline log data in the mud-rich intervals, we show that overpressure is generated by unloading mechanisms, probably including both gas generation and clay mineral diagenesis, and not disequilibrium compaction. Our interpretation is radically different from that of previous workers, who have all concluded that the principal mechanism for generating overpressure was disequilibrium compaction.

In the following sections, we give background on the geology of the basin, overpressure distribution, and wireline log responses to overpressure before presenting our analysis of log, pressure, temperature, and vitrinite reflectance data. We then discuss the implications for overpressure generation mechanisms and, in reaching our conclusions, comment on the particular circumstances in the Lower Kutai Basin which make it a rewarding basin to study for understanding overpressure generation and chemical compaction in mud-rich sedimentary successions.

Geological background and overpressure distribution

Tectonically, the Lower Kutai Basin has experienced several episodes of rift, sag, and inversion resulting from interaction between the Eurasia plate to the north, the Pacific Plate to the east, and the Australian Plate to the south (Moss & Chambers 1999). The main inversion episodes have occurred from the Middle Miocene to the present, and have been responsible for the development of anticlinal structures (Chambers *et al*. 2004). The major structural

feature is the Samarinda Anticlinorium, consisting of a series of anticlines and synclines with axes oriented approximately north–south. This anticlinorium is highly folded and faulted on the onshore area, whereas dips are gentle in the shallow water and deep offshore areas. The main north–south anticlinal folds are the Onshore Axis, Internal Axis, Median Axis, External Axis, and Offshore Axis (Fig. 1). The Peciko Field is located on the Median Axis.

According to Allen & Chambers (1998), the thickness of the Neogene section in the basin, which comprises deltaic sediment sourced by the Mahakam River in eastern Kalimantan, may reach about 14 km in the depocentre. The Mahakam Delta is a fluvial-tidal mud-dominated delta that has been prograding from the Early Miocene to the present day. Stratigraphically, the productive interval in the Middle–Upper Miocene succession is the Tunu Main Zone, and the hydrocarbons present are mainly gas. The Tunu Main Zone is sub-divided into six intermediate stratigraphic units, of which only the uppermost five are present in the Peciko Field. They have an average thickness of 300–400 m, based on the presence of third-order maximum flooding surfaces. The intermediate stratigraphic units are further sub-divided into several smaller stratigraphic units, based on the presence of local flooding surfaces. The reservoirs in this field are dominantly distributary mouth bars (Samson *et al.*, 2005). The dimensions of individual mouth bars are 1–3 m thick and 1500–4000 m wide, and stacked mouth bars attain thicknesses of 10–30 m (Fig. 2a). Figure 2b is a schematic cross-section of the field which illustrates the stacked nature of the gas reservoirs and the tilted gas-water contacts in the deeper overpressured accumulations.

The burial history of the Tunu Main Zone in this field (Fig. 3) shows that the sedimentation rate during the last 8 My has been fairly constant at around 300 m My^{-1}. This ongoing deposition of fine-grained sediment has previously been interpreted as being

101 responsible for the generation of overpressure by disequilibrium compaction in this area (Bois
102 *et al*. 1994; Bates 1996; Burrus 1998).
103
104 The inversion episodes have caused almost all of the Neogene sedimentary layers to
105 crop out in the onshore and coastal areas. Consequently, overpressure can bleed off laterally
106 on the basin scale, depending on the degree of reservoir connectivity. This process is known
107 as lateral reservoir drainage (O'Connor & Swarbrick 2008). The occurrence of lateral
108 reservoir drainage in the Peciko Field was identified by Grosjean *et al*. (1994) and Lambert *et*
109 *al*. (2003). The lateral overpressure gradients are sufficiently large to create hydrodynamic
110 traps for gas. For example, in stratigraphic unit 3 the lateral overpressure gradient reaches 150
111 psi km^{-1} (Fig. 4a). Given a gas density of 0.2 g cm^{-3}, the gas-water contact has a tilt of up to
112 7°. There is ample field evidence of tilted accumulations of gas in the deeper reservoir
113 intervals of the Peciko Field. In these reservoirs, the gas accumulations are displaced down-
114 dip on to the northern flank of the structure, as shown schematically in Fig. 2b, and the gas
115 column in crestal wells is either very thin or absent (Fig. 4b). A south–north cross-section
116 (Fig. 5) shows that both top of overpressure and the top of the pressure transition zone deepen
117 to the north, where the strata are more sand-rich.
118
119 Information about source rocks in the Lower Kutai Basin generally, and in the Peciko
120 Field specifically, has been provided by Oudin & Picard (1982), Schoell *et al*. (1985), Burrus
121 *et al*. (1992), Paterson *et al*. (1997), Duval *et al*. (1998), and Lambert *et al*. (2003). The main
122 source rocks in the area are organic-rich mudrocks, coal beds, and even sandy facies
123 deposited in fluvial, deltaic top, tidal plain, and delta front settings. They are mostly classified
124 as Type III source rocks. Although the organic-rich mudrocks are gas prone, Lambert *et al*.
125 (2003) reported that the oil-generative potential of the Type III organic matter is unusually

high. The contribution to hydrocarbon generation from marine mudrocks, located in the deepwater Makassar Straits and in the deeper part of fields surrounding Mahakam Delta, is thought to be negligible because their organic content is low. Interestingly, isotopic analysis performed by Lambert *et al*. (2003) showed that the threshold for both gas and oil maturation corresponds to a vitrinite reflectance of 0.6%.

Wireline log responses to overpressure

There are several candidate mechanisms for generating overpressure in the Lower Kutai Basin, including disequilibrium compaction, clay diagenesis, gas generation, and lateral pressure transfer. Wireline log analysis can help to distinguish between these mechanisms (e.g. Bowers 2001; Katahara 2006).

When a mud-rich sedimentary succession cannot dewater rapidly enough for the pore pressure to remain hydrostatic during burial, its porosity is greater than that it would be if the pore pressure were hydrostatic, and the overpressure is said to be caused by disequilibrium compaction. Where overpressure has been generated by disequilibrium compaction in a uniform mudrock succession, with virtually no loss of pore fluid, the porosity remains constant and the pore pressure-depth profile becomes parallel to the vertical stress-depth profile.

Where overpressure has been generated by an unloading mechanism such as clay diagenesis, gas generation or lateral transfer, the pore pressure can increase more rapidly with depth than the vertical stress (Fig. 6). In such circumstances, the density usually continues to increase with depth through the overpressured mudrocks, while the sonic log trend reverses, moving towards higher sonic travel time with increasing depth. The resistivity log trend also

reverses, moving towards lower resistivity with increasing depth. These responses can be explained by the concept of storage pores and connecting pores (Bowers & Katsube 2002). When pore pressure in a mudrock increases due to fluid expansion, the unloading response is essentially elastic and results in only a very small increase in porosity. Because the density log measures the bulk porosity of the mudrock, it is barely affected by the fluid expansion. The increase in porosity that does occur during fluid expansion is predominately due to the opening of flat connecting pores, because they are more compliant than the storage pores. The sonic and resistivity log responses are sensitive to the opening of connecting pores because their opening reduces the bulk modulus and rigidity and increases the conductivity.

Data analysis

The Peciko Field was developed using the concept of hydrodynamic trapping (Grosjean *et al*. 1994; Lambert *et al*. 2003), and a campaign of reservoir pressure measurements for hydrodynamic analysis purposes has resulted in an excellent pressure database. On average, there are around 70 RFT points in each well. These pressure data are very useful for overpressure analysis because they can be used both to determine overpressure distribution and to calibrate methods of pore pressure estimation.

We have analysed data from the discovery well, PEC-1, and 16 appraisal wells in the Peciko Field, most of which have terminated at the pressure transition zone into hard overpressure. Here, we present data from three wells, PEC-1, NWP-9, and NWP-16 (Fig. 2a), to illustrate our findings. PEC-1 was chosen as a typical example of a well on the crest of the structure and because source rock maturation data are available from it, although it does contain a relatively small number of RFT points and no density log was run in this early well. NWP-9 was chosen because it encounters the highest overpressure value in the Peciko Field

and shows a clear unloading response on density-sonic and density-resistivity crossplots. NWP-16 is located downflank in the northern part of the field where the top of overpressure is deeper and the geothermal gradient is slightly lower (Fig. 3). It is the deepest well in the field and was chosen to make a comparison of the wireline log responses with those from well NWP-9.

Prior to analysing the wireline response to overpressure, it is necessary to discriminate mud-rich intervals from more silty and sandy intervals from the given set of wireline logs. Discrimination was done by cross-plotting density against the difference between neutron porosity and the porosity estimated from the density logs (Fig. 7), as done by Katahara (2006). To infer porosity from the density log, a matrix density of 2.75 g cm^{-3} and a fluid density of 1.05 g cm^{-3} were arbitrarily assumed. An arbitrary threshold value of 0.18 was chosen (i.e., NPHI – DPHI > 0.18) to ensure that our pressure analysis was consistently performed in the mud-rich intervals, although tests showed that estimated pore pressures in the mudrocks had low sensitivity to the choice of threshold value.

The pressure-depth plot for well PEC-1 (Fig. 8a) is typical of wells in this field, except that the top of overpressure is located at slightly greater depths further north (Fig. 3). The overpressure initially increases slowly with depth below the top of overpressure at ~9500 ft (~2900 m) and then more rapidly through a transition zone into hard overpressure. The top of the transition zone is at ~11,300 ft (~3450 m). The top of transition zone is picked at the depth where vertical effective stress starts to decrease as depth increases.

According to Lambert *et al.* (2003), the maturity threshold for gas generation corresponds to a vitrinite reflectance value of 0.6%. Well PEC-1 is the only well in the

Peciko Field from which vitrinite reflectance data are available (Fig. 8b). There is a correlation between the top of the transition zone into hard overpressure and the vitrinite reflectance value of 0.6%. Four data points in the interval 10,000–12,000 ft (3050–3650 m) have vitrinite reflectance values below the general trend. There is no other available information to indicate whether they are reliable, but there is a possibility that these values were obtained from fragments due to caving, and not cuttings from the drill bit.

The pressure-depth plot for well NWP-9 (Fig. 9) indicates that the top of overpressure is at a depth of ~11,000 ft (~3350 m), although there is a good RFT measurement showing ~300 psi (~2 MPa) of overpressure in an isolated sand body at ~10,000 ft (~3050 m) depth. The top of the transition into hard overpressure is around 12,000 ft (3650 m) depth, where reversals can be seen in the trends of both the sonic and resistivity logs through the mudrocks. The density log, by contrast, shows no obvious reversal, but it shows consistently high values of density, around 2.6 g cm^{-3}, in the depth interval 11,000–13,000 ft (3350–3950 m).

The pressure-depth plot for well NWP-16 (Fig. 10) appears to converge slightly towards the lithostatic gradient with increasing depth, but it is not clear whether the well has entered the expected transition zone into hard overpressure. The wireline logs appear to display asymptotic trends towards the bottom of the well, without any clear indication of reversals, although it is possible that the trends of both sonic and resistivity logs are on the point of reversing at the bottom of the well.

Crossplots of density against sonic and resistivity log values for mudrocks in well NWP-9 are shown in Fig. 11, with data points colour-coded at intervals of 1000 ft (305 m). The smectitic and illitic compaction trends, introduced by Dutta (2002) and adopted by

Katahara (2006), are shown on the density-sonic crossplot for reference. The smectitic compaction trend is followed by mudrocks with a high proportion of discrete smectite. The illitic compaction trend is followed by mudrocks in which all the discrete smectite has been transformed into mixed-layer illite/smectite. Both crossplots show clear unloading responses starting at a depth of ~12,000 ft (~3650 m). The data points coloured red in the deepest interval show changes in trend, with increased sonic transit time and decreased resistivity but no decrease in density. These observations provide clear evidence that the generating mechanism for hard overpressure is an unloading process. Data points in the depth range 5000–12,000 ft (1500–3650 m) on the density-sonic crossplot fall on, or close to, the illitic compaction trend. The average geothermal gradient is around 0.0094 °C ft^{-1} (0.031°C m^{-1}) with a surface temperature of 30°C, giving an estimated temperature of nearly 80°C at 5000 ft (1500 m) depth, sufficient for discrete smectite to have disappeared (Hower *et al*. 1976; Boles & Franks 1979).

Clauer *et al*. (1999) investigated clay mineralogy in the Tunu Field, which is located on the Median Axis north of Peciko (Fig. 1) so the clay mineralogy in the two fields may be expected to be similar. At sampling depths below 7700 ft (2350 m), they found that the clay fraction consists of mixed-layer illite/smectite, kaolinite/dickite, detrital illite and chlorite. This clay mineral composition is consistent with the illitic compaction trend observed below ~5000 ft (~1500 m) (Fig. 11). The fact that the density-sonic crossplot follows an illitic compaction trend over the hydrostatically pressured depth interval of 5000–11,000 ft (1500–3350 m) indicates that excess water which may have been released by the transformation of discrete smectite to mixed-layer illite/smectite has dissipated and does not contribute to present-day overpressures. However, clay diagenetic reactions that continue to be active at higher temperatures, including ongoing illitization of mixed-layer illite/smectite and the

conversion of kaolinite to illite (Bjørlykke 1998), and also quartz dissolution and precipitation (Bjørkum 1995), probably do contribute to present-day overpressures.

Composite density plots for mudrocks in all 16 NWP wells (Fig. 4a) are shown in Fig. 12, without and with the data points from the overpressured intervals in each well. The density continues to increase smoothly below the top of overpressure, even though the vertical effective stress reaches its maximum value at the top of overpressure in each well. Thus, compaction appears to continue with increasing depth, independent of the vertical effective stress. This plot constitutes strong evidence for ongoing chemical compaction below the top of overpressure, and for discounting disequilibrium compaction as a mechanism that contributes to the generation of overpressure in this field. Given the high average density, in excess of 2.6 g cm^{-3} below 12,000 ft in all wells (Fig. 12), our preferred interpretation is that the mudrocks in the overpressured intervals have become overcompacted by diagenetic processes, i.e. overcompacted in a mechanical sense due to the chemical compaction processes.

Implications for overpressure generation

Pressure-depth plots show that the top of overpressure is at depths of 9500–12,000 ft (2900–3650 m), corresponding to estimated temperatures of 120–140°C, and that there is a transition zone into hard overpressure at depths of 11,500–14,000 ft (3500–4250 m), corresponding to estimated temperatures of 140–160°C. These depths to the top of overpressure are relatively large in comparison to other Neogene basins worldwide, as summarized by Swarbrick *et al.* (2002). For example, in the Malay Basin where the sedimentation rate is around 800 ft My^{-1} (240 m My^{-1}), about 20% less than the sedimentation rate over the last 8 My in the Lower Kutai Basin, the top of overpressure is around 3200 ft (975 m) depth. Presumably, the top of

overpressure in the Lower Kutai Basin is so deep because of lateral reservoir drainage (Grosjean *et al*. 1994; Lambert *et al*. 2003). Inversion started in Middle Miocene times and has continued to the present day with uplift centred on the onshore area (Chambers *et al*. 2004). Unpublished net-to-gross (NTG) maps for the Median Axis region of the Lower Kutai Basin show a progressive upward increase in NTG at the Peciko Field from stratigraphic unit 5 up to stratigraphic unit 3 (Figs 2b and 5), which is consistent with effective lateral drainage above the overpressured zone.

Within the transition zone into hard overpressure in well NWP-9, both density-sonic and density-resistivity crossplots show clear unloading responses (Figs 9 and 11). Clay diagenesis may contribute to the present-day overpressure in the Peciko Field. In the hydrostatically pressured succession, data on the density-sonic crossplots lie on the illite-rich compaction trend below ~5000 ft (~1500 m), and remain on this trend in the zone of low overpressure (Fig. 10). Although discrete smectite is likely to have disappeared by 5000 ft (1500 m) burial depth, where the temperature approaches 80°C, illitization of mixed-layer illite/smectite is ongoing at greater depths to much higher temperatures (Hower *et al*. 1976; Boles & Franks 1979). Kaolinite transforms to illite at temperatures ~130–140°C in basin settings (Bjørlykke 1998) and can contribute to overpressure both through the release of free water by the reaction and by transferring load from the grains to the pore fluid as mineral grains are dissolved (Bjørlykke & Hoeg 1997). This temperature range roughly corresponds to that estimated at the depth of the transition zone into high overpressure. Furthermore, the dissolution of kaolinite and precipitation of illite may reduce porosity and permeability at this depth, and thereby help to maintain high overpressure in the deeper strata.

Gas generation seems likely to be another unloading process responsible for the hard overpressure, generated both directly from kerogen and from oil cracking to gas. According to Lambert *et al*. (2003), gas generation starts at a vitrinite reflectance of 0.6%. We have one set of vitrinite reflectance data in the Peciko Field, i.e. in PEC-1 where there is a correlation between high overpressure and vitrinite reflectance values above 0.6% (Fig. 7). Oudin & Picard (1982) found that there is a good correlation between the top of hard overpressure and the increase in vitrinite reflectance in the Handil Field (Fig. 13), and Bates (1996) found a similar correlation in the Nilam Field (Fig. 14). However, they did not draw any conclusions about overpressure generation mechanisms from the vitrinite reflectance data. We note that the data in each of those two wells show a strong correlation between the depth of transition into hard overpressure and the onset of gas generation, assuming that the threshold for gas generation corresponds to a vitrinite reflectance of 0.6%.

To the south and east of the Peciko Field, the sands within the Tunu Main Zone peter out as the depositional environment changes from the shelf break setting to deep marine. Since the organic carbon content of the deep marine sediment is low and its potential for hydrocarbon generation is negligible, there is unlikely to be significant lateral transfer of overpressure generated by gas generation in the synclinal area to the southeast, but there may be lateral transfer of overpressure generated by diagenetic reactions.

In all wells with density logs, NWP-1 to NWP-16, the logged density values continue gradually to increase downwards through the zone of low overpressure (Fig. 12), which is consistent with ongoing chemical compaction. The top of overpressure is located deep within the chemical compaction zone, where the effective stress appears to have no influence on compaction and the mudrocks are likely to be stiffened by chemical compaction so that they

are overconsolidated (Bjørlykke & Hoeg 1997; Bjørlykke 1998, 1999). Consequently, we attribute the origin of the low overpressures, above the transition zone into hard overpressure, to passive transmission of pore fluid from the highly overpressured zone below.

Conclusions

Hard overpressure in the Peciko Field is generated by unloading mechanisms. The top of overpressure is much deeper than the depth range where transformation of discrete smectite to mixed-layer smectite/illite occurs, so the disappearance of smectite does not contribute to the observed overpressure. The causes of the hard overpressure in the Peciko Field are likely to be gas generation, illitization of mixed-layer illite/smectite, conversion of kaolinite to illite, and dissolution and precipitation of quartz. We suggest that expulsion of fluid resulting from gas generation and diagenesis in the zone of high overpressure maintains the hydrodynamic flow through the reservoir layers containing gas accumulations.

Compaction continues below the top of overpressure, independent of vertical effective stress, in all 16 wells where density logs have been run. This observation is clear evidence of ongoing chemical compaction. The origin of the low overpressure above the transition zone into high overpressure is probably due to vertical transfer from below. The transition zone into hard overpressure can be recognized from sonic and resistivity log reversals, whether by direct inspection of the logs or by crossplotting their responses against the density log.

The high mudrock densities, greater than 2.6 g cm^{-3}, at the top of overpressure indicate that the mudrocks are overcompacted. Therefore, our preferred interpretation is that disequilibrium compaction does not contribute to the overpressure. This conclusion is radically new because all other studies of overpressured Neogene basins have suggested that

disequilibrium compaction has contributed to the overpressure, either directly or indirectly by pressure transference. The particular circumstances in the Lower Kutai Basin which make our interpretation plausible are that it is a warm basin with lateral reservoir drainage. Consequently, the top of overpressure is unusually deep for a mud-rich sequence that has undergone rapid burial over the last 10 My.

Acknowledgements

We thank Total Indonesie for funding and data and Guillaume Smagghe for ongoing support and a critical review. However, the views expressed are those of the authors and not necessarily those of Total Indonesie. We benefited from discussions with Richard Swarbrick and very constructive reviews by Gunn Teige and Quentin Fisher.

References

Allen, G. P. & Chambers, J. L. C. 1998. *Sedimentation in the Modern and Miocene Mahakam Delta*. Field Trip Guide Book, Indonesian Petroleum Association, Jakarta.

Bates, J. A. 1996. Overpressuring in the Kutai Basin: distribution, origins, and implications for the petroleum system. *In: Indonesian Petroleum Association, Proceedings 25th Annual Convention*, 93-115.

Bjørkum, P. A. 1995. How important is pressure in causing dissolution of quartz in sandstones? *Journal of sedimentary Research*, **66**, 147-154.

374 Bjørlykke, K. 1998. Clay mineral diagenesis in sedimentary basins: a key to the prediction of
375 rock properties: examples from the North Sea Basin. *Clay Minerals*, **33**, 15–34.
376
377 Bjørlykke, K. 1999. Principal aspects of compaction and fluid flow in mudstones. *In:* Aplin,
378 A.C., Fleet, A.J. & Macquaker, J.H.S. (eds) *Muds and Mudstones: Physical and Fluid-Flow*
379 *Properties*. Geological Society, London, Special Publications, **158**, 73-78.
380
381 Bjørlykke, K. & Høeg, K. 1997. Effects of burial diagenesis on stresses, compaction and fluid
382 flow in sedimentary basins. *Marine and Petroleum Geology*, **14**, 267-276.
383
384 Bois, M., Grosjean, Y. & de Pazzis, L. 1994. Shale compaction and abnormal pressure
385 evaluation application to the offshore Mahakam. *In: Indonesian Petroleum Association,*
386 *Proceedings 23rd Annual Convention*, 245-259.
387
388 Boles, J. R. & Franks, S. G. 1979. Clay diagenesis in Wilcox sandstones of southwest Texas:
389 implications of smectite diagenesis on sandstone cementation. *Journal of Sedimentary*
390 *Petrology*, **49**, 55-70.
391
392 Bowers, G. L. 1995. Pore pressure estimation from velocity data: accounting for overpressure
393 other than undercompaction. *SPE Drilling & Completion*, **10**(2), 89-95.
394
395 Bowers, G. L. 2001. Determining an appropriate pore-pressure estimation strategy. *Offshore*
396 *Technology Conference*, paper OTC 13042.
397

398 Bowers, G. L. & Katsube, T. J. 2002. The role of shale pore structure on the sensitivity of
399 wire-line logs to overpressure. *In:* Huffman, A.R. & Bowers, G.L. (eds), *Pressure Regimes in*
400 *Sedimentary Basins and their Prediction.* AAPG, Tulsa, Memoir **76**, 43-60.
401
402 Burrus, J. 1998. Overpressure models for clastic rocks, their relation to hydrocarbon
403 expulsion: a critical reevaluation. *In:* Law, B.E., Ulmishek, G.F. & Slavin, V.I. (eds)
404 *Abnormal Pressures in Hydrocarbon Environments*. AAPG, Tulsa, Memoir **70**, 35-63.
405
406 Burrus, J., Brosse, E., Choppin de Janvry, G., Grosjean, Y. & Oudin, J. L. 1992. Basin
407 modelling in the Mahakam Delta based on integrated 2D model Temispack. *In: Indonesian*
408 *Petroleum Association, Proceedings 21st Annual Convention*, 23-43.
409
410 Chambers, J. L. C., Carter, I., Cloke, R., Craig, J., Moss, S. J. & Paterson, D. W. 2004. Thin-
411 skinned and thick-skinned inversion-related thrusting – a structural model for the Kutai Basin,
412 Kalimantan, Indonesia. *In:* McClay, K.R. (ed.) *Thrust Tectonics and Hydrocarbon Systems*.
413 AAPG, Tulsa, Memoir **82**, 614-634.
414
415 Clauer, N., Rinckenbach, T., Weber, F., Sommer, F., Chaudhuri, S. & O'Neil, J. R. 1999.
416 Diagenetic evolution of clay minerals in oil-bearing Neogene sandstones and associated
417 shales, Mahakam Delta Basin, Indonesia. *AAPG Bulletin*, **83**, 62-87.
418
419 Dutta, N. C. 2002. Deepwater geohazard prediction using prestack inversion of large offset P-
420 wave data and rock model. *The Leading Edge*, **21**, 193-198.
421

422 Duval, B. C., Cassaigneau, C., Choppin de Janvry, G., Loiret, B., Leo, M., Alibi & Grosjean,
423 Y. 1998. Impact of the petroleum system approach to exploration and appraisal efficiency in
424 the Mahakam Delta. *In: Indonesian Petroleum Association, Proceedings 26th Annual*
425 *Convention*, 277-290.
426
427 Grosjean, Y., Choppin de Janvry, G. & Duval, B. C. 1994. Discovery of a giant in a mature
428 deltaic province: Peciko, Indonesia. Presented at the 14th World Petroleum Congress, May–
429 June 1994, Stavanger, Norway.
430
431 Hermanrud, C., Wensaas, L., Teige, G. M. G., Vik, E., Nordgård Bolås, H. M. & Hansen, S.
432 1998. Shale porosities from well logs on Haltenbanken (Offshore Mid-Norway) show no
433 influence of overpressuring. *In:* Law, B.E., Ulmishek, G.F. & Slavin, V.I. (eds.) *Abnormal*
434 *Pressures in Hydrocarbon Environments*. AAPG, Tulsa, Memoir **70**, 65-87.
435
436 Hower, J., Eslinger, E. V., Hower, M. E. & Perry, E. A. 1976. Mechanism of burial and
437 metamorphism of argillaceous sediment : 1. Mineralogical and chemical evidence. *Geological*
438 *Society of America Bulletin*, **87**, 725-737.
439
440 Katahara, K. 2006. Overpressure and shale properties: stress unloading or smectite-illite
441 transformation? *76th SEG Annual Meeting*, Expanded Abstracts, 1520-1524.
442
443 Lambert, B., Duval, B. C., Grosjean, Y., Umar, I. M. & Zaugg, P. 2003. The Peciko case
444 history: impact of an evolving geological model on the dramatic increase of gas reserves in
445 the Mahakam Delta. *In:* Halbouty, M.T. (ed.) *Giant Oil and Gas Fields of the Decade 1990–*
446 *1999*. AAPG, Tulsa, Memoir **78**, 297-320.

Moss, S. J. & Chambers, J. L. C. 1999. Depositional modelling and facies architecture of rift and inversion episodes in the Kutai Basin, Kalimantan, Indonesia. *In: Indonesian Petroleum Association, Proceedings 27th Annual Convention*, 467-486.

O'Connor, S. A. & Swarbrick, R. E. 2008. Pressure regression, fluid drainage and a hydrodynamically controlled fluid contact in the North Sea, Lower Cretaceous, Britannia Sandstone Formation. *Petroleum Geoscience*, **14**, 115-126.

Oudin, J. L. & Picard, P. F. 1982. Genesis of hydrocarbons in Mahakam Delta and the relationship between their distribution and the overpressured zone. *In: Indonesian Petroleum Association, Proceedings 11th Annual Convention*, 181-202.

Paterson, D. W., Bachtiar, A., Bates, J. A., Moon, J. A. & Surdam, R. C. 1997. Petroleum system of the Kutei Basin, Kalimantan, Indonesia. *In: Indonesian Petroleum Association, Proceedings Petroleum Systems of SE Asia and Australasia Conference*, 709-726.

Pennebaker, E. S. 1968. Seismic data indicate depth and magnitude of abnormal pressure. *World Oil*, **166**, 73-82.

Reynolds, E. B. 1970. Predicting overpressure zones with seismic data. *World Oil*, **171**, 78-82.

Samson, P., Dewi-Rochette, T. & Lescoeur, M. 2005. Peciko geological modeling: optimizing fluid distribution and model resolution of a giant gas field in a shale-dominated deltaic environment. Asia Pacific Oil & Gas Conference, SPE paper 93253.

Schoell, M. B., Durand, B. & Oudin, J. L. 1985. Migration of oil and gas in the Mahakam Delta: evidence and quantitative estimate from isotope and biomarker studies. *In: Indonesian Petroleum Association, Proceedings 14th Annual Convention*, 49-56.

Swarbrick, R. E., Osborne, M. J. & Yardley, G. S. 2002. Comparison of overpressure magnitude resulting from the main generating mechanisms. *In:* Huffman, A.R. & Bowers, G.L. (eds) *Pressure Regimes in Sedimentary Basins and their Prediction*. AAPG, Tulsa, Memoir **76**, 1-12.

Teige, G. M. G., Hermanrud, C., Wensaas, L. & Nordgård Bolås, H. M. 1999. The lack of relationship between overpressure and porosity in North Sea and Haltenbanken shales. *Marine and Petroleum Geology*, **16**, 321-335.

Teige, G. M. G., Hermanrud, C., Wensaas, L. & Nordgård Bolås, H. M. 2007. Geological constraints of pore pressure detection in shales from seismic data. *Basin Research*, **19**, 33-50.

Tingay, M. R. P., Hillis, R. R., Swarbrick, R. E., Morley, C. K. & Damit, A. R. 2009. Origin of overpressure and pore-pressure prediction in the Baram province, Brunei. *AAPG Bulletin*, **83**, 51-74.

Figure captions

Figure 1. Major structural features in the Lower Kutai Basin. The main north–south anticlines are indicated by the outlines of known hydrocarbon accumulations.

Figure 2. Schematic sections through the Peciko Field at different vertical scales: (a) stacked mouth bars in a stratigraphic interval between two local flooding surfaces (after Samson et al., 2005); and (b) gas accumulations (red) with tilted GWCs in the Tunu Main Zone. SU1–SU5 are stratigraphic units of the Tunu Main Zone. A simplified lithological column for SU3 is shown on the right: yellow denotes sand-rich intervals and green mudrock intervals.

Figure 3. Burial history of the Tunu Main Zone in the Peciko Field (modified from Lambert *et al*. 2003).

Figure 4. (a) Lateral overpressure distribution in the uppermost reservoir of stratigraphic unit 3 in the Peciko Field before production started. Pressure data were taken from the discovery well, PEC-1, and the 16 NWP appraisal wells. Overpressure contours are at intervals of 50 psi. The outline of the field indicates the lateral extent of gas accumulations in all units. (b) Pore fluid distribution in the same stratigraphic unit showing that the gas accumulation is located on the north flank of the structure. Red line: limit of the gas accumulation in this stratigraphic unit. Red circles: wells where the reservoir is gas-bearing. Blue circles: wells where this reservoir contains only water. Circle diameter is proportional to reservoir layer thickness in each well. Structural contour interval is 82 ft (25 m).

519 Figure 5. South–north vertical section through the Peciko Field along the line marked in Fig.
520 4a showing the general trend of overpressure with depth.
521
522 Figure 6. Pressure-depth plot (right) with sonic and density log responses expected for a
523 mudrock succession where overpressure is generated by an unloading process. Below the top
524 of overpressure, the reversal in the trend of sonic transit time does not indicate abnormally
525 high porosity because density continues to increase with depth.
526
527 Figure 7. Crossplot of density against the difference between neutron and density porosities
528 estimated from wireline logs in well NWP-9. NPHI – DHPI = 0.18 was arbitrarily chosen as
529 the mudrock cut-off.
530
531 Figure 8. (a) Pressure-depth plot for well PEC-1. (b) Vitrinite reflectance data showing that
532 the threshold value of 0.6 % for gas generation, as determined by Lambert *et al.* (2003),
533 coincides with the top of the transition zone into hard overpressure. The encircled data points
534 are outliers from the trend and so may contain errors.
535
536 Figure 9. Pressure-depth plot for well NWP-9 with density, sonic, and resistivity log data for
537 the mudrocks.
538
539 Figure 10. Pressure-depth plot for well NWP-16 with density, sonic, and resistivity log data
540 for the mudrocks.
541
542 Figure 11. Crossplots of density against sonic transit time and resistivity for well NWP-9.
543 Data points on unloading trends are encircled in blue.

544

545 Figure 12. Composite density plot for mudrocks, defined by NPHI – DPHI > 0.18, in all the
546 NWP wells, Peciko Field: (a) for the hydrostatically pressured intervals only; and (b) for all
547 the density log data.

548

549 Figure 13. Vitrinite reflectance data and the pressure-depth plot from well H-9-B1 in the
550 Handil Field (location in Fig. 1). After Oudin & Picard (1982).

551

552 Figure 14. Vitrinite reflectance data from well N-109X in the Nilam Field (location in Fig. 1)
553 After Bates (1996).

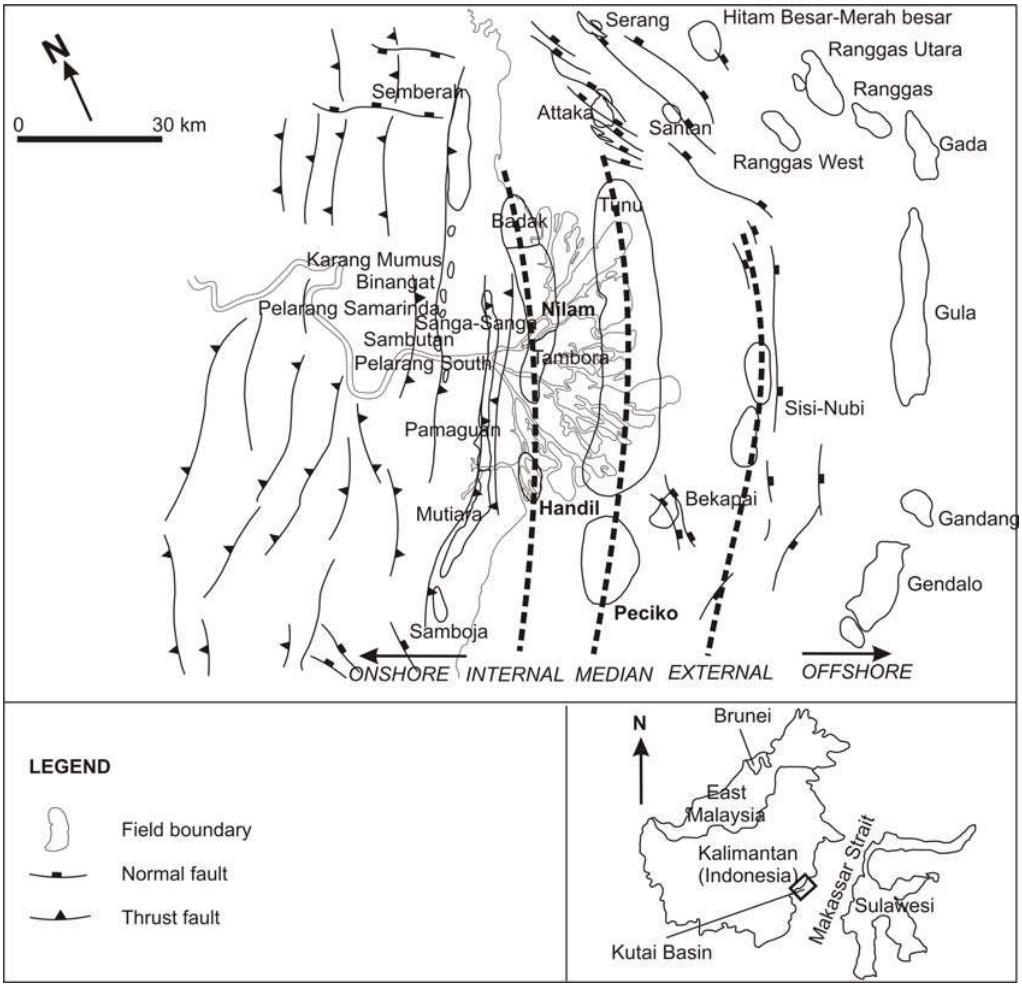

Figure 1. Major structural features in the Kutai Basin. The main north–south anticlines are indicated by the outlines of known hydrocarbon accumulations.

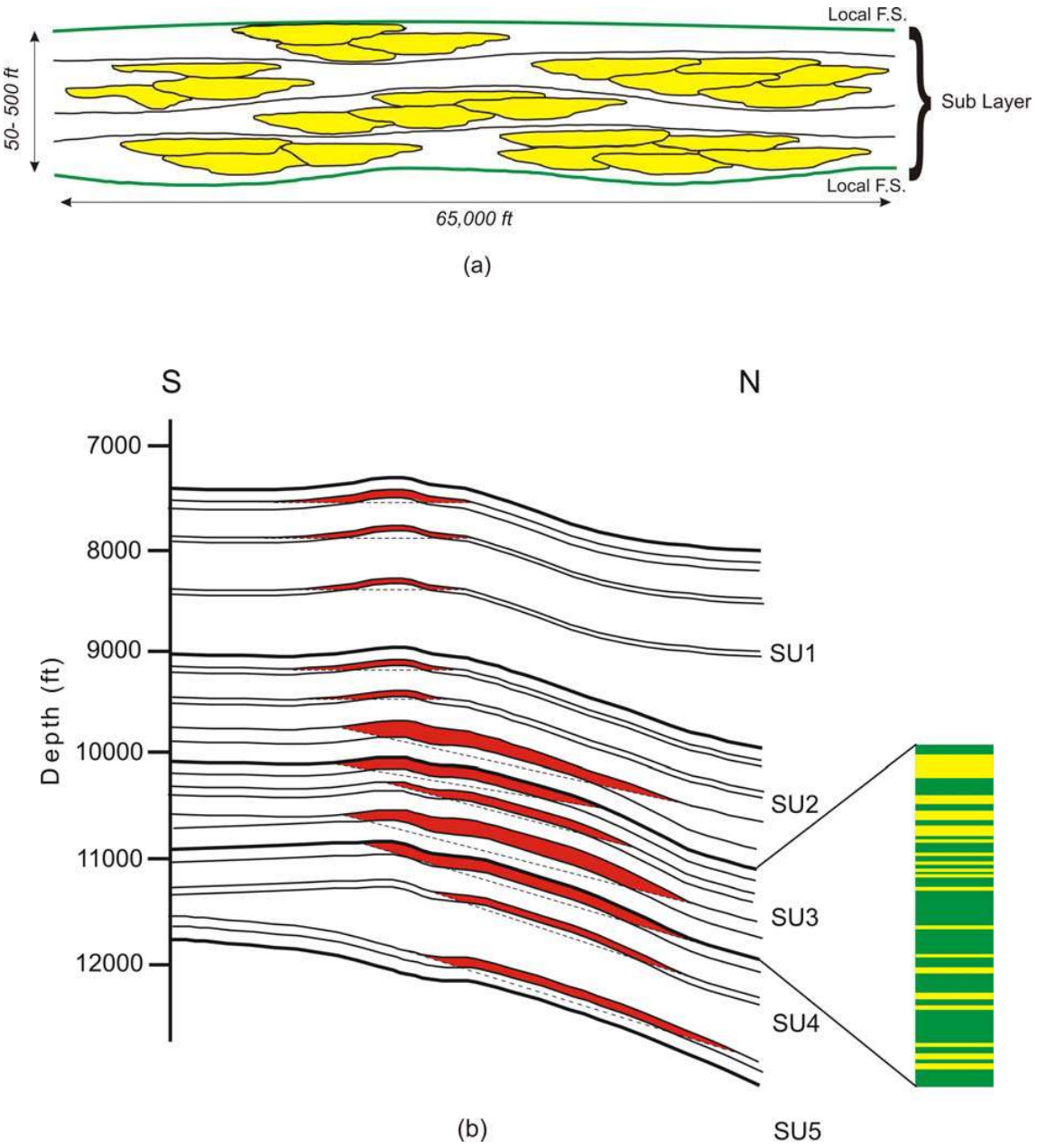

Figure 2. Schematic sections through the Peciko Field at different vertical scales: (a) stacked mouth bars in a stratigraphic interval between two local flooding surfaces (after Samson et al., 2005); and (b) gas accumulations (red) with tilted GWCs in the Tunu Main Zone. SU1–SU5 are stratigraphic units of the Tunu Main Zone. A simplified lithological column for SU3 is shown on the right: yellow denotes sand-rich intervals and green mudrock intervals.

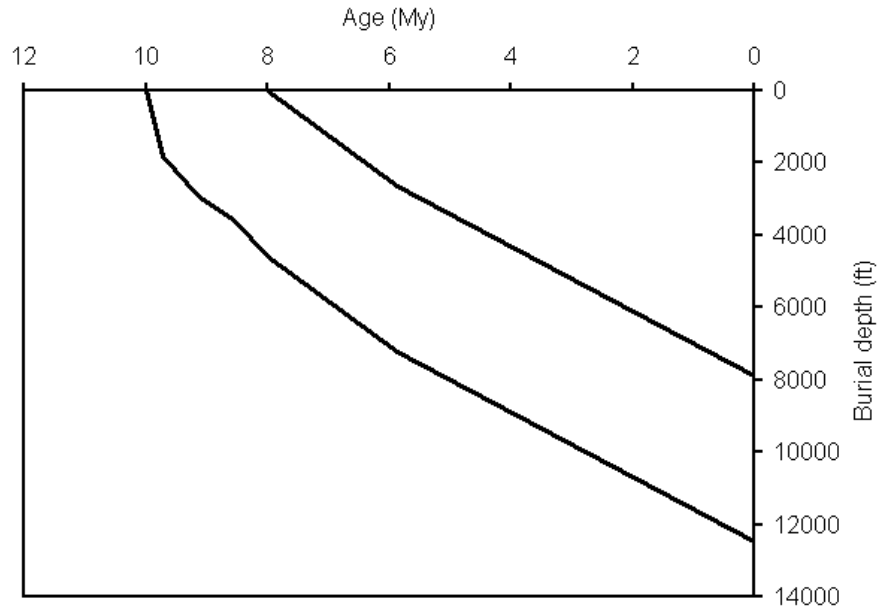

Figure 3. Burial history of Tunu Main Zone in the Peciko Field (modified from Lambert *et al*. 2003).

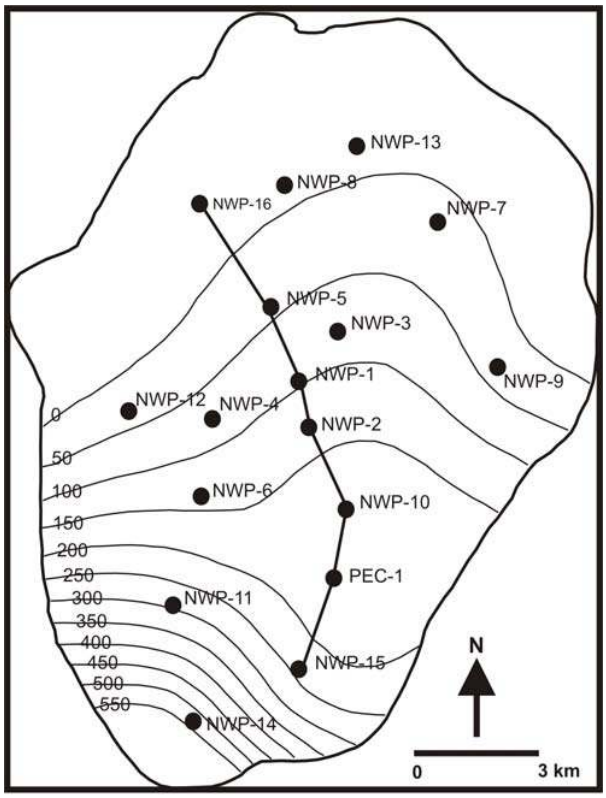
NWP-13
NWP-8
NWP-16
NWP-7
NWP-5
NWP-3
NWP-1
NWP-9
NWP-12
NWP-4
NWP-2
0
50
100
150
200
250
300
350
400
450
500
550
NWP-6
NWP-10
PEC-1
NWP-11
NWP-15
NWP-14
N
0
3 km

(a)

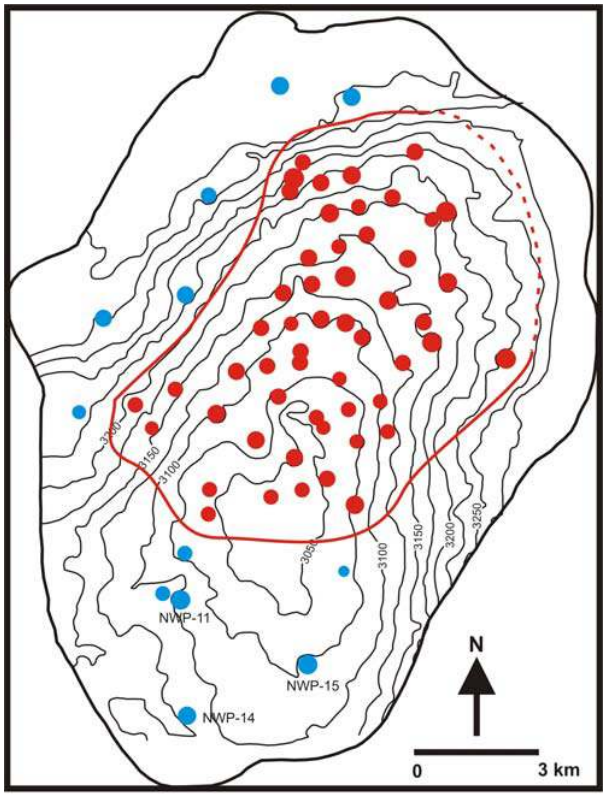
3200
3150
3100
3050
3100
3150
3200
3250
NWP-11
NWP-15
NWP-14
N
0
3 km

(b)

Figure 4. (a) Lateral overpressure distribution in the uppermost reservoir of stratigraphic unit 3 in the Peciko Field before production started. Pressure data were taken from the discovery well, PEC-1, and the 16 NWP appraisal wells. Overpressure contours are at intervals of 50 psi. The outline of the field indicates the lateral extent of gas accumulations in all units. (b) Pore fluid distribution in the same stratigraphic unit showing that the gas accumulation is located on the north flank of the structure. Red line: limit of the gas accumulation in this stratigraphic unit. Red circles: wells where the reservoir is gas-bearing. Blue circles: wells where this reservoir contains only water. Circle diameter is proportional to reservoir layer thickness in each well. Structural contour interval is 82 ft (25 m).

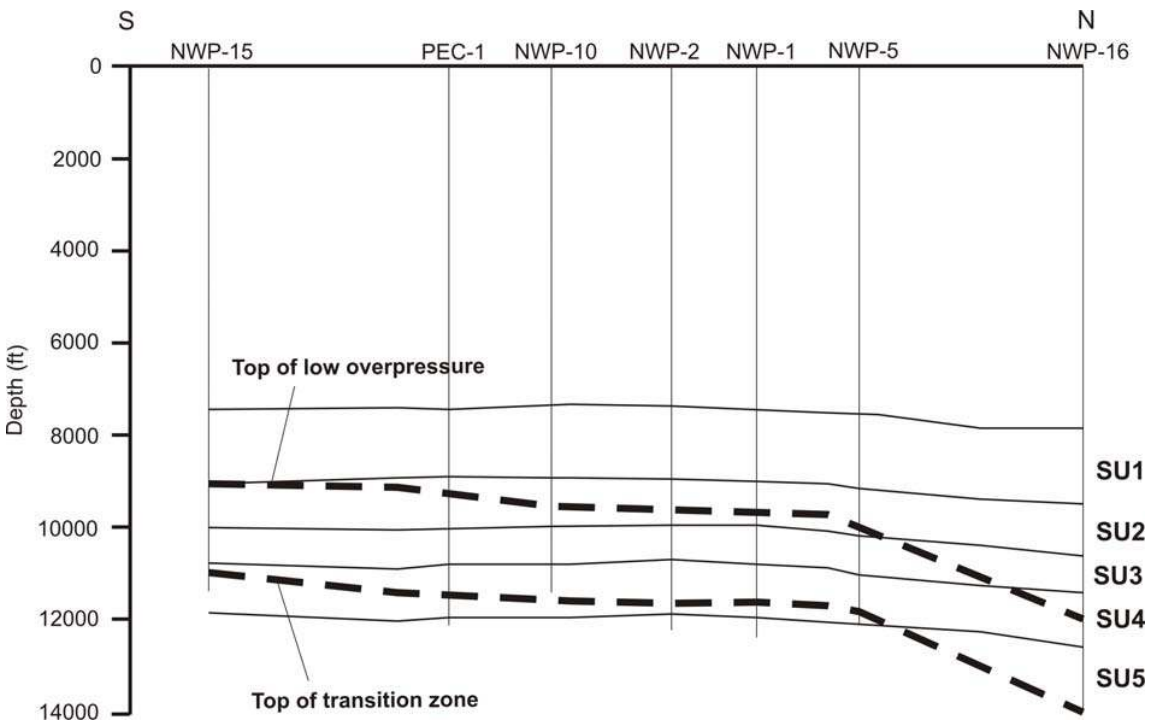

Figure 5. South–north vertical section through the Peciko Field along the line marked in Fig. 4a showing the general trend of overpressure with depth.

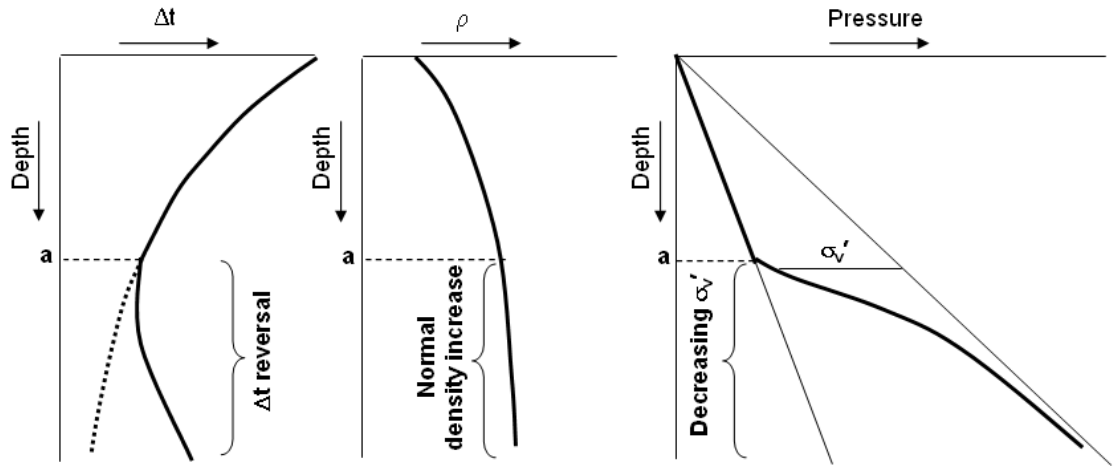

Figure 6. Pressure-depth plot (right) with sonic and density log responses expected for a mudrock succession where overpressure is generated by an unloading process. Below the top of overpressure, the reversal in the trend of sonic transit time does not indicate abnormally high porosity because density continues to increase with depth.

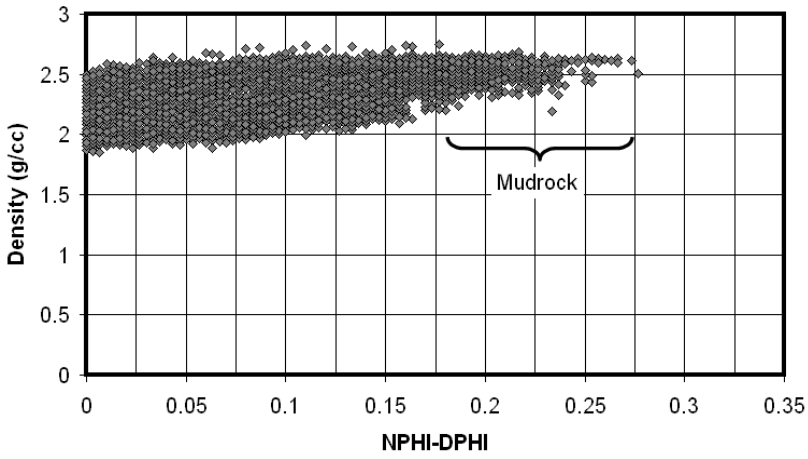

Figure 7. Crossplot of density against the difference between neutron and density porosities estimated from wireline logs in well NWP-9. NPHI – DHPI = 0.18 was arbitrarily chosen as the mudrock cut-off.

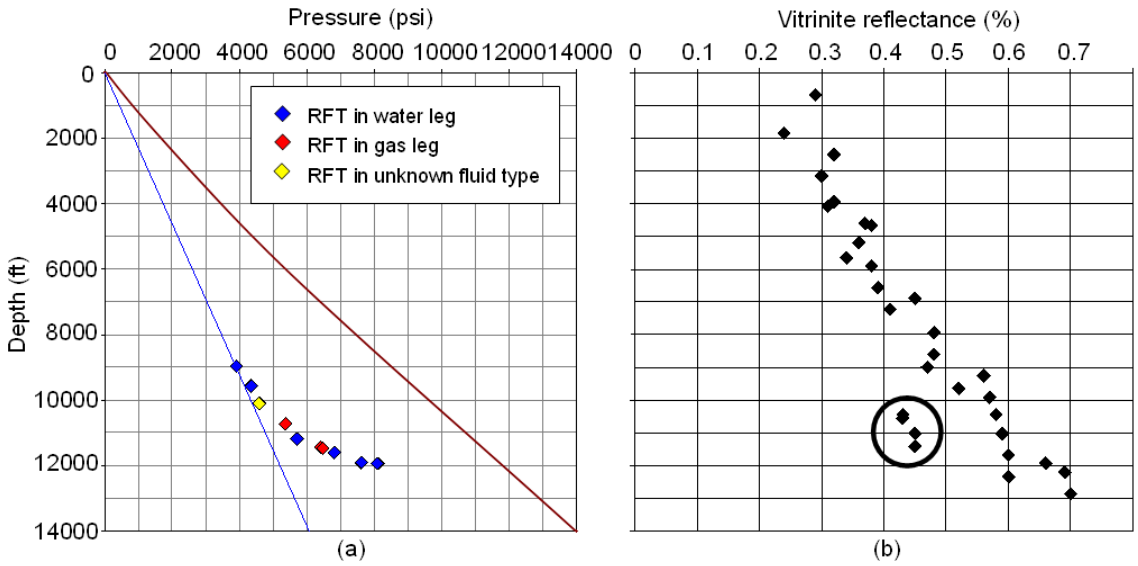

Figure 8. (a) Pressure-depth plot for well PEC-1. (b) Vitrinite reflectance data showing that the threshold value of 0.6 % for gas generation, as determined by Lambert *et al*. (2003), coincides with the top of the transition zone into hard overpressure. The encircled data points are outliers from the trend and so may contain errors.

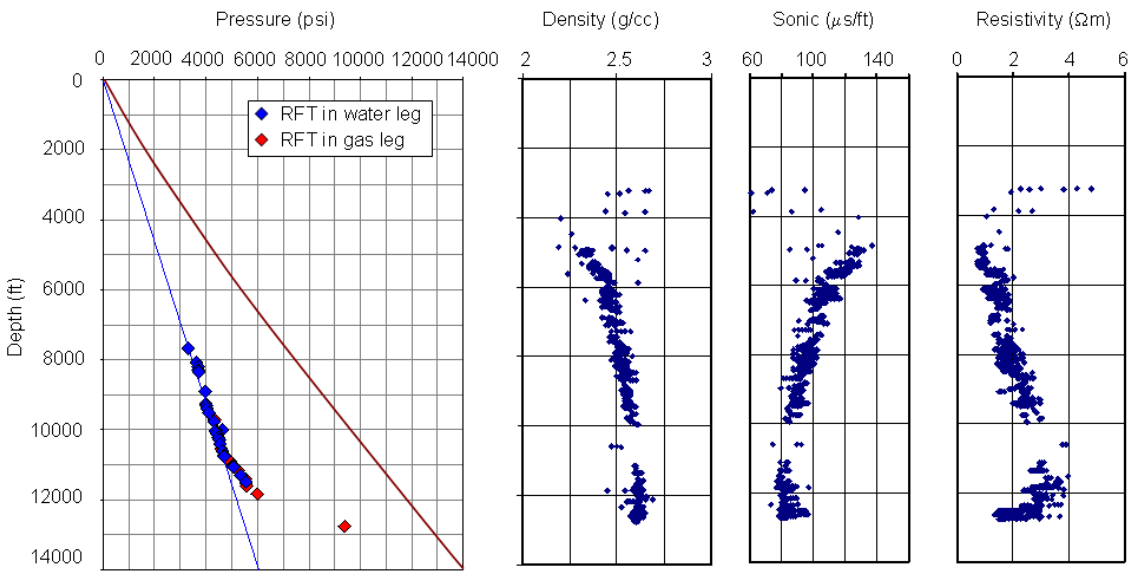

Figure 9. Pressure-depth plot for well NWP-9 with density, sonic, and resistivity log data for the mudrocks.

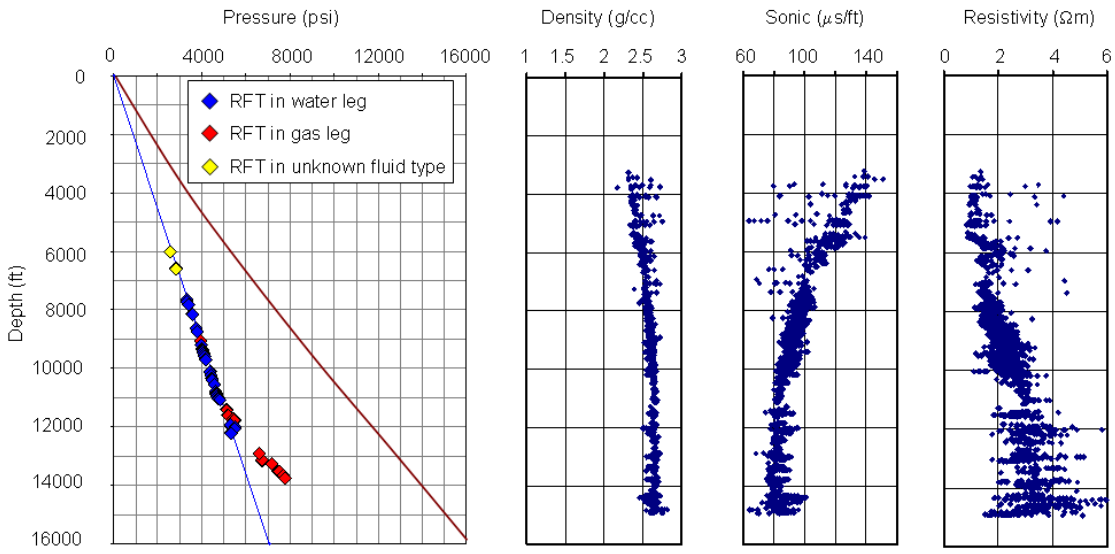

Figure 10. Pressure-depth plot for well NWP-16 with density, sonic, and resistivity log data for the mudrocks.

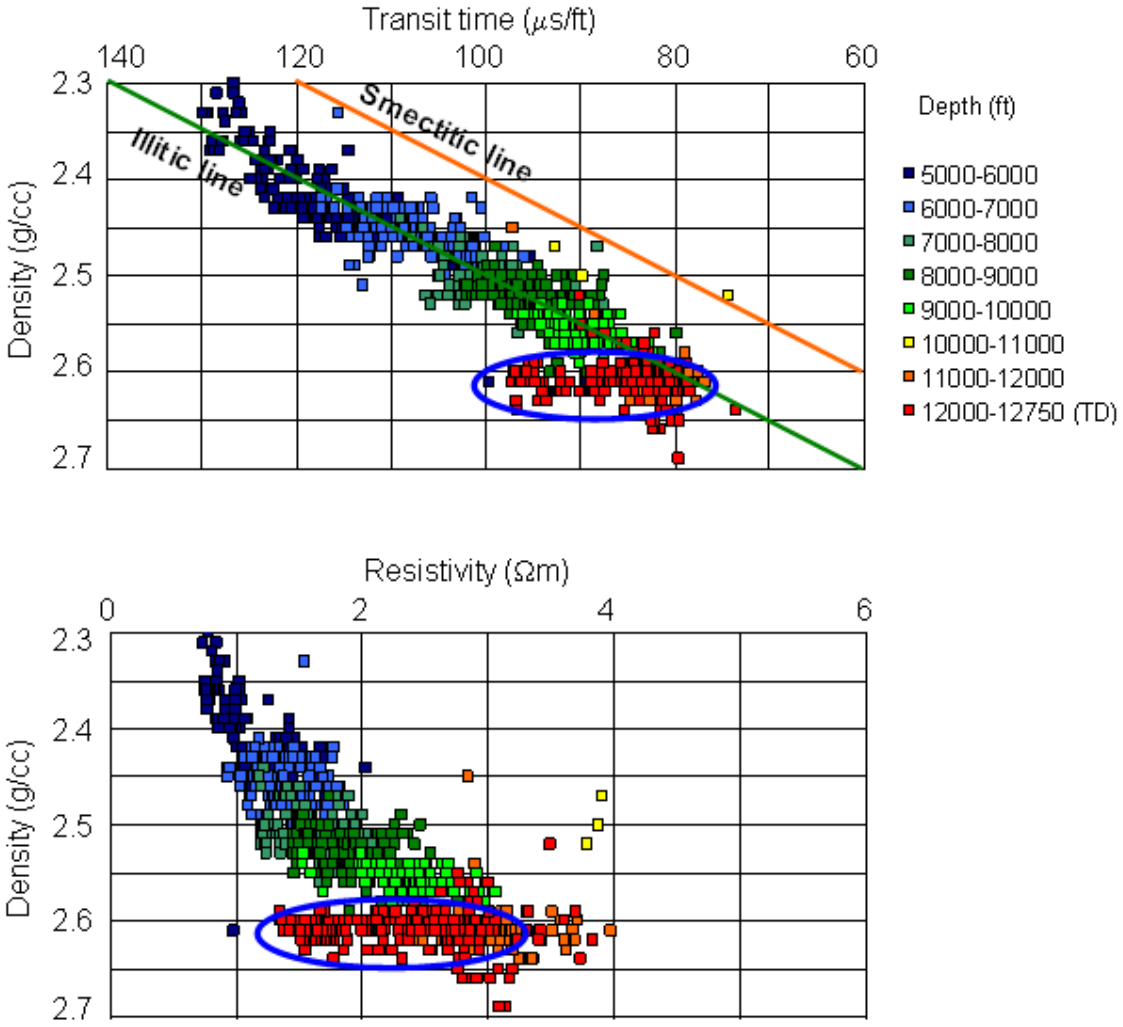

Figure 11. Crossplots of density against sonic transit time and resistivity for well NWP-9.

Data points on unloading trends are encircled in blue.

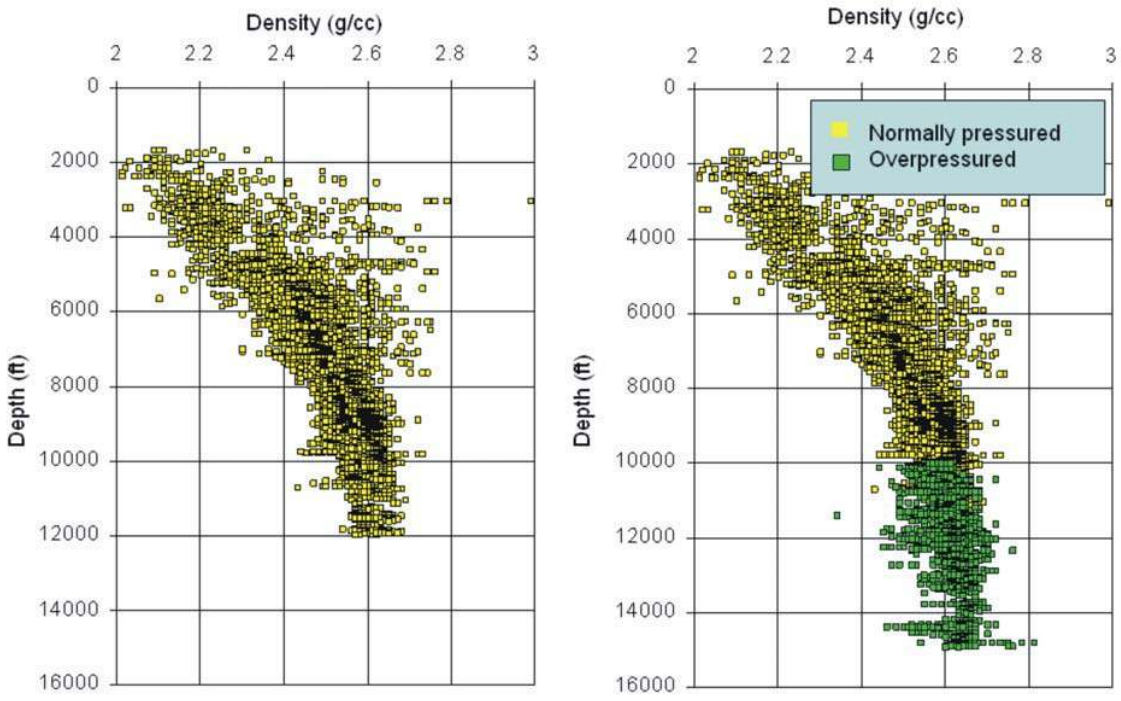

Figure 12. Composite density plot for mudrocks, defined by NPHI – DPHI > 0.18, in all the NWP wells, Peciko Field: (a) for the hydrostatically pressured intervals only; and (b) for all the density log data.

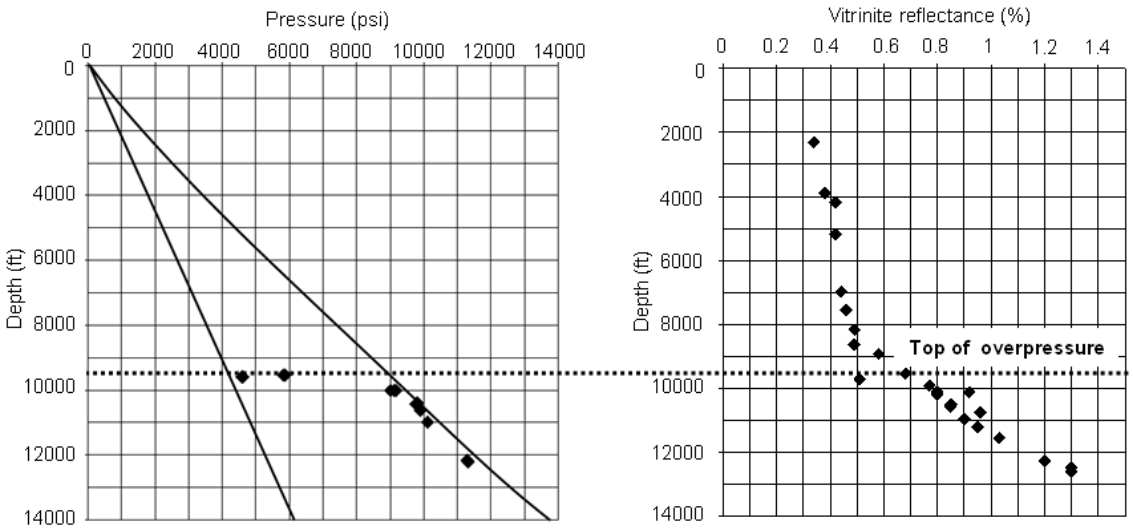

Figure 13. Vitrinite reflectance data and the pressure-depth plot from well H-9-B1 in the Handil Field (location in Fig. 1). After Oudin & Picard (1982).

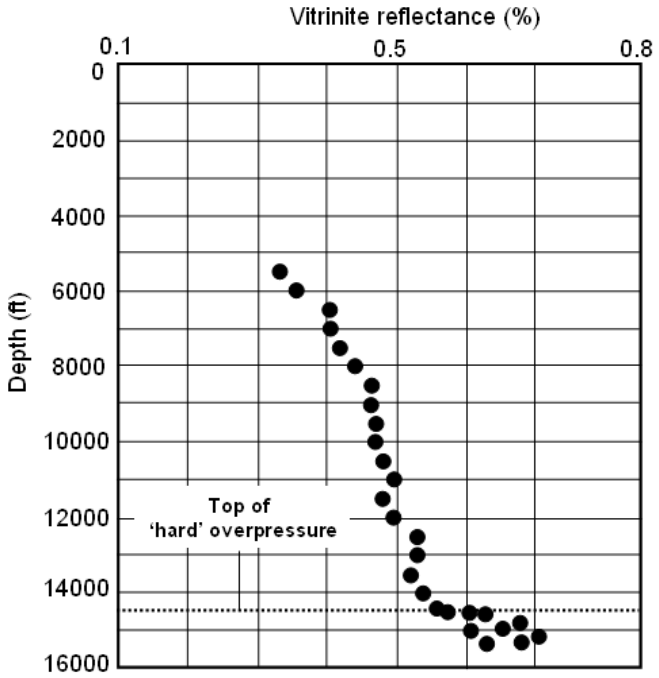

Figure 14. Vitrinite reflectance data from well N-109X in the Nilam Field (location in Fig. 1) After Bates (1996).